Nuclear Science and Techniques (2026) 37:85
https://doi.org/10.1007/s41365-026-01899-1

Design of a 500 MHz TM_{020}-mode cavity with elliptical choke for the high-current Super Tau-Charm Facility

Cheng-Zhe Wang[1] · Ye-Long Wei[1] · Li Sun[1] · Tian-Long He[1] · Yuan-Cheng Xie[1] · Zhi-Cheng Huang[1] · Yi-Hao Zhang[1] · Meng-Xu Fan[1] · Luigi Faillace[2] · David Alesini[2]

Received: 26 July 2025 / Revised: 26 August 2025 / Accepted: 30 September 2025

Abstract
A compact TM_{020}-mode RF cavity was proposed and studied by KEK and RIKEN for the storage ring of the NanoTerasu facility. However, performance limitations due to accelerating mode leakage into the coaxial slots have been identified. This paper presents an improved TM_{020}-mode cavity design to solve this issue. By employing an elliptical choke, the leakage power can be significantly reduced. Harmful parasitic modes other than the TM_{020}-mode are effectively suppressed using the elliptical choke placed at the magnetic node of the TM_{020}-mode. Through optimization, this improved TM_{020}-mode RF cavity meets the requirements of the Super Tau-Charm Facility (STCF) collider rings with a beam current of up to 2 A. Detailed mechanical design and thermal analysis confirm the feasibility and stability of the improved cavity.

Keywords TM_{020}-mode · Normal-conducting RF cavity · Elliptical choke · Leakage power · Super Tau-Charm Facility

1 Introduction

Radiofrequency (RF) cavities are widely utilized for delivering power to the beam, accelerating the charged particles, and compensating for synchrotron radiation losses in different accelerator facilities, such as synchrotron radiation sources [1–5] and colliders [6–10]. The Super Tau-Charm Facility (STCF) is an electron–positron collider that has been proposed and studied by the Chinese particle physics community [10, 11]. It is designed to operate in a center-of-mass energy range from 2 to 7 GeV with a peak luminosity of 0.5×10^{35} $cm^{-2} \cdot s^{-1}$ or higher. The STCF project is currently under development with an extensive R&D program, including the RF system. To meet the requirements of collider ring physics, the RF system must provide an accelerating voltage of 6 MV and a beam power of 3 MW for each ring. A TM_{020}-mode normal-conducting (NC) cavity was selected as a candidate for the RF system of the collider ring because such a cavity has a low R/Q [12].

The TM_{020}-mode RF cavities operating at TM_{020}-mode were initially proposed by researchers at KEK and RIKEN and successfully commissioned for the storage ring of NanoTerasu [13]. Compared to conventional TM_{010}-mode cavities, the TM_{020}-mode cavity exhibits a higher unloaded quality factor Q_0 and a lower R/Q [4, 14]. This characteristic helps reduce the required detuning frequency, significantly suppressing the coupled-bunch instabilities (CBIs) driven by the accelerating mode [15].

The distinctive symmetrical electromagnetic field distribution of the TM_{020}-mode enables the ferrites to be directly embedded into coaxial slots inside the cavity, as illustrated in Fig. 1 instead of using special waveguides or pipes. This damping scheme not only heavily suppresses all harmful parasitic modes without affecting the accelerating TM_{020}-mode, but also reduces the longitudinal spaces, making the cavity extremely compact. However, the introduction of a high-power input coupler and other components may disrupt the symmetry of the electromagnetic field, leading to leakage power of the accelerating mode into the coaxial

This work was supported by the "Hundred Talents Program" of the Chinese Academy of Sciences (No. KJ2310007003), the Fundamental Research Funds for the Central Universities (Nos. WK2310000114, KY2310000047, and KY2310000067), and the Chinese Academy of Sciences President's International Fellowship Initiative (No. 2025PD0102) and Super Tau-Charm Facility key technology research project.

✉ Ye-Long Wei
wylong@ustc.edu.cn

[1] National Synchrotron Radiation Laboratory, University of Science and Technology of China, Hefei 230029, China

[2] INFN Frascati National Laboratories, Frascati, Rome, Italy

Published online: 12 February 2026

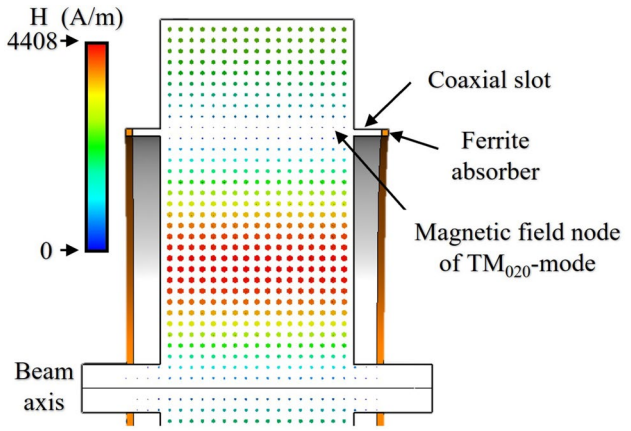

Fig. 1 (Color online) Magnetic field distribution of TM_{020}-mode in TM_{020}-mode RF cavity

slots and absorption by ferrites. Additionally, machining errors in the position of the coaxial slots may result in a large leakage power of the accelerating mode. The leakage power causes a reduction in the unloaded quality factor Q_0 of the accelerating mode and a heating issue for the ferrites, significantly limiting the RF performance of the TM_{020}-mode cavity [16].

To address the leakage issue, Li et al. [5] proposed a method to compensate for electromagnetic field distortion by introducing a geometrically optimized tab structure at the coaxial coupling port, thereby reducing the leakage rate to below 1%. The leakage rate is defined as the ratio of the power loss of the accelerating mode absorbed by the ferrites to the power dissipated on the cavity wall. Similarly, Yamaguchi et al. [16] developed a novel loop-type coupler to mitigate the perturbation of the electromagnetic field, achieving a leakage rate of less than 1%. These approaches effectively resolve the leakage issues associated with coaxial couplers. However, when a waveguide coupler is employed in a TM_{020}-mode cavity, leakage power remains an issue.

This study proposes a solution to resolve the power leakage issue in a TM_{020}-mode cavity with a waveguide input coupler. By employing an elliptical choke, the leakage of the accelerating mode was significantly reduced, and the mechanical structure was simplified. Section 2 introduces the theory of the choke. Section 3 analyzes the issues related to leakage power and provides the elliptical choke design in detail. Section 4 describes the design of the frequency tuners. Section 5 presents the suppression of the harmful parasitic modes. Section 6 presents the multipacting analysis. Section 7 presents the thermomechanical analysis of the cavity. Section 8 concludes the paper.

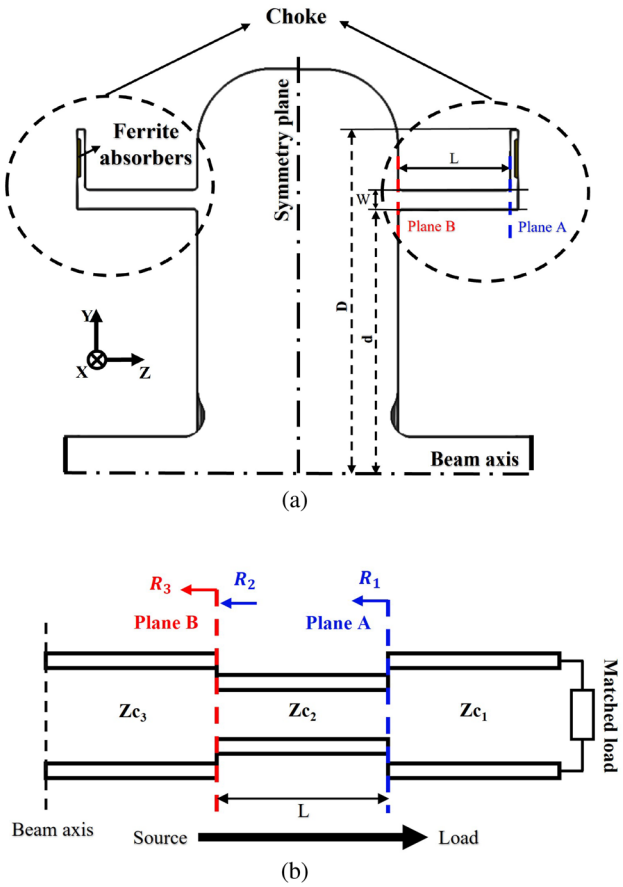

Fig. 2 (Color online) A TM_{020}-mode cavity with choke (**a**), and the equivalent model of transmission lines (**b**), where L, W, D, and d represent the length, width, outer radius, and inner radius of the choke geometry; Zc_1, Zc_2, Zc_3 represent the characteristic impedances of each of the transmission lines, and R_1, R_2, R_3 represent the reflection coefficients at different planes

2 Theory of choke

The choke-mode accelerating geometry was initially proposed by Shintake et al. [17]. The principle is that the choke reflects the accelerating mode, whereas the harmful parasitic modes pass through the choke and are absorbed by the load. Based on this concept, Zha et al. proposed an improved X-band choke-mode damped structure for the main linac of the Compact Linear Collider (CLIC) [18], achieving nearly complete dipole damping and significantly reducing the total transverse kicks. Inspired by these developments, a choke can be introduced into the TM_{020}-mode cavity with a waveguide input coupler to address the issue of leakage power.

As shown in Fig. 2a, the choke geometry can be regarded as a set of coaxial transmission lines strategically positioned at the magnetic field node of the TM020-mode inside the cavity, instead of being arranged along the radial direction of the outer wall. This particular placement takes

advantage of the electromagnetic field distribution of the TM_{020}-mode, allowing the choke to selectively reflect the accelerating mode while allowing the harmful parasitic modes to be absorbed. Through optimization of the choke, the leakage power of the accelerating mode can be significantly reduced, and the harmful parasitic modes can be effectively suppressed.

The choke can be equivalently modeled as a series combination of two uniform, lossless coaxial transmission lines, each characterized by its own characteristic impedance, as shown in Fig. 2b

$$Zc = 60\ln\left(\frac{R_{\text{out}}}{R_{\text{in}}}\right)(\Omega), \tag{1}$$

where R_{out} and R_{in} represent the outer and inner radii of the coaxial section. Using the dimensions of the choke geometry, we obtained the characteristic impedances $Zc_1 = 60\ln\left(\frac{D}{d}\right)$ and $Zc_2 = 60\ln\left(\frac{d+W}{d}\right)$. Zc_3 represents the characteristic impedance at the slot position inside the cavity, and it can be calculated as follows.

As shown in Fig. 2b, the end of the coaxial transmission line was terminated with ferrites. This can be modeled as a perfectly matched load with a normalized characteristic impedance of 1. The transmission line, with two different characteristic impedances at each end, is connected in series at plane A. Consequently, the reflection coefficient at plane A is calculated using the following equation:

$$R_1 = \frac{\frac{Zc_1}{Zc_2} - 1}{\frac{Zc_1}{Zc_2} + 1}. \tag{2}$$

The RF wave propagates from plane A to plane B, and a phase shift $\phi = \frac{2\pi L}{\lambda}$ is obtained, where λ is the free space wavelength. Thus, the reflection coefficient R_2 at plane B is expressed as:

$$R_2 = R_1 \exp\left(-2j\phi + \theta_0\right), \tag{3}$$

where θ_0 is the initial phase of the wave.

Similar to the reflection coefficient R_1, the reflection coefficient R_3 at plane B is calculated as:

$$R_3 = \frac{\frac{Zc_2}{Zc_3}\cdot\frac{1+R_2}{1-R_2} - 1}{\frac{Zc_2}{Zc_3}\cdot\frac{1+R_2}{1-R_2} + 1}. \tag{4}$$

By substituting R_3 into Eq. (4), the characteristic impedance Zc_3 can be obtained. R_3 is determined by the ratio of reflected power P_{ref} and input power P_{in} at plane B:

$$R_3 = \sqrt{\frac{P_{\text{ref}}}{P_{\text{in}}}}. \tag{5}$$

The input power can be divided into reflected power and power dissipated in the load:

$$P_{\text{in}} = P_{\text{ref}} + P_{\text{load}}. \tag{6}$$

Then, we have:

$$P_{\text{load}} = P_{\text{in}}\left(1 - R_3^2\right), \tag{7}$$

where P_{load} is the power absorbed by the load, P_{in} is the input power to the choke, and R_3 is the reflection coefficient at plane B. The absorbed power P_{load} is related to the quality factor of the resonant cavity as follows:

$$Q_0 = \frac{\omega U}{P_{\text{c}}}, \tag{8}$$

$$Q_{\text{load}} = \frac{\omega U}{P_{\text{c}} + P_{\text{load}}}, \tag{9}$$

where Q_0 and Q_{load} are the quality factors without and with a matched load, respectively; ω is the angular frequency; U is the stored energy in the cavity; and P_{c} is the power loss on the cavity surface.

Then, we have:

$$P_{\text{load}} = \omega U\left(\frac{1}{Q_{\text{load}}} - \frac{1}{Q_0}\right). \tag{10}$$

By varying the choke length L to change the phase shift ϕ, Q_{load} can be directly simulated from ANSYS HFSS [19] as a function of L, with a fixed choke width $W = 25$ mm, as shown in Fig. 3 (denoted by the dotted black curve). Two arbitrary points (Q_{load1}, L_1) and (Q_{load2}, L_2) are selected for

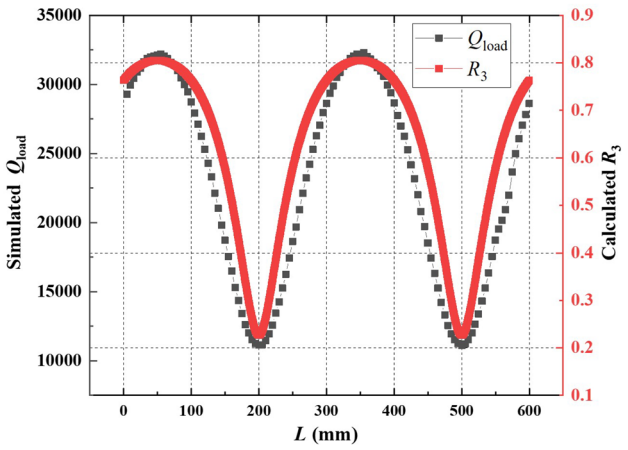

Fig. 3 (Color online) Simulated Q_{load} and calculated R_3 as a function of choke length L

Eqs. (7) and (10). The corresponding reflection coefficients R_{31} and R_{32} satisfy the following relationship:

$$\frac{1-|R_{31}|^2}{1-|R_{32}|^2}=\frac{\frac{1}{Q_{\text{load1}}}-\frac{1}{Q_0}}{\frac{1}{Q_{\text{load2}}}-\frac{1}{Q_0}}. \tag{11}$$

Combining Eqs. (4) and (11), the value of Z_{c3} is obtained. This Z_{c3} is then substituted back into Eq. (4) to calculate the reflection coefficient R_3 as a function of the choke length L, as shown in Fig. 3 (denoted as the dotted red curve). It can be observed that there is a good agreement between the calculated R_3 and simulated Q_{load}, validating the proposed transmission line model. The reflection coefficient R_3 reaches its maximum at

$$L=50\,\text{mm}+n\frac{\lambda}{2},\quad n=1,2,3\ldots, \tag{12}$$

with a fixed choke width $W=25\,\text{mm}$. At these points, the TM_{020}-mode is strongly reflected back into the cavity, effectively reducing the leakage power.

To reduce the leakage power of the accelerating mode while suppressing harmful parasitic modes, the influence of the choke width W is evaluated. By sweeping different choke widths W, calculations are performed with the aim to minimize the absorption rate $P_{\text{load}}/P_{\text{in}}$ for the TM_{020}-mode and minimize R_3 for other harmful modes including TM_{010}-mode, TM_{021}-mode, TM_{030}-mode, TM_{031}-mode, and TM_{040}-mode. As shown in Fig. 4, the absorption rate $P_{\text{load}}/P_{\text{in}}$ for the accelerating TM_{020}-mode gradually increases when the choke width W rises. In contrast, the reflection coefficients R_3 for the harmful parasitic modes show a significant reduction, particularly in the range of $W=20\sim30$ mm. A choke width in this range represents a compromise between the strong suppression of harmful parasitic modes and the minimum leakage rate for the accelerating mode. This provides a theoretical basis for the geometric design of the elliptical choke in the following sections.

3 Design and analysis

Owing to the distinctive symmetrical electromagnetic field distribution of the TM_{020}-mode, the coaxial slots must be positioned at the radial node of the magnetic field so that all harmful parasitic modes are strongly damped without affecting the accelerating mode. However, the introduction of an input coupler and frequency tuners may induce localized perturbations to the TM_{020}-mode, thereby disrupting the symmetry of the field distribution. In this situation, some partial power of the accelerating mode leaks into the coaxial slots and is absorbed by the ferrites. This reduces the unloaded quality factor Q_0 of the accelerating mode and increases the heating load on the ferrites. The frequency tuner effect can be solved by using multiple structures for symmetrical distribution. This is described in Sect. 4.

To investigate the asymmetrical electromagnetic field distribution of the TM_{020}-mode caused by the introduction of the coupler, cavities with and without a waveguide input coupler were simulated using ANSYS HFSS [19], as shown in Fig. 5.

As shown in Fig. 6a, the node of magnetic field for the TM_{020}-mode is a symmetrical circle inside a cavity without

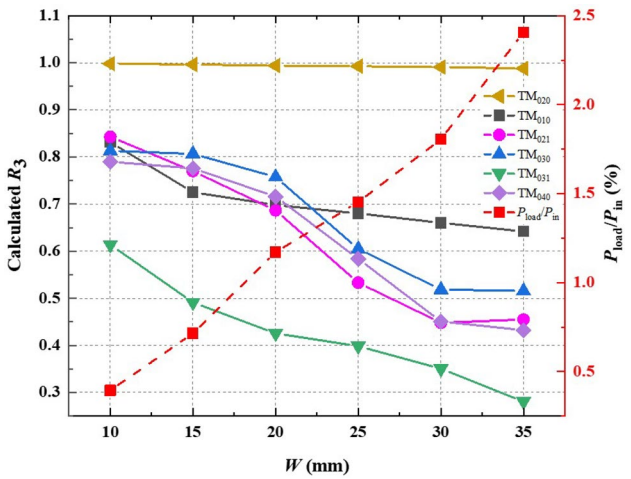

Fig. 4 (Color online) Calculated R_3 for the accelerating TM_{020}-mode and selected harmful parasitic modes (TM_{010}-mode, TM_{021}-mode, TM_{030}-mode, TM_{031}-mode, and TM_{040}-mode) and the absorption rate $P_{\text{load}}/P_{\text{in}}$ for the accelerating TM_{020}-mode as a function of choke width W

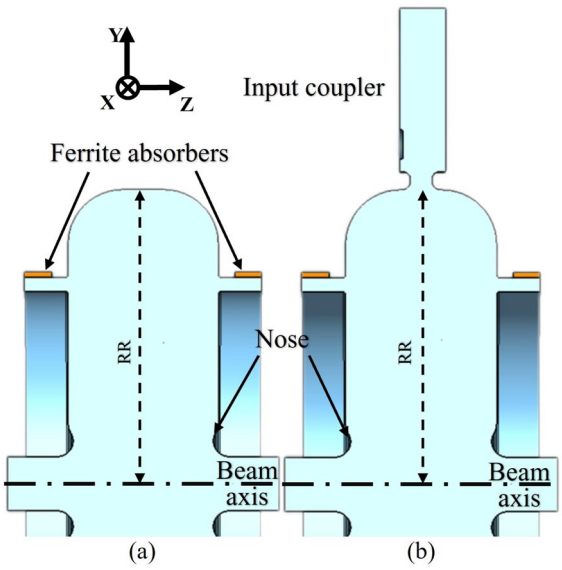

Fig. 5 (Color online) Geometry of two TM_{020}-mode cavity models: **a** without an input coupler; **b** with a waveguide input coupler

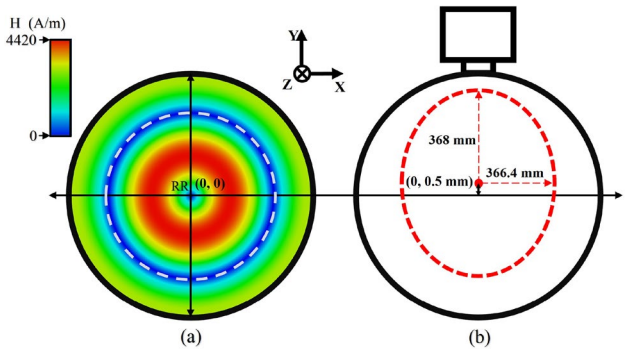

Fig. 6 (Color online) Magnetic field distribution of the TM_{020}-mode (**a**), and deformation of the TM_{020}-mode magnetic field node (**b**). The white dashed line represents the simulated shape of the TM_{020}-mode magnetic field node without an input coupler, while the red dashed line represents the node with a waveguide input coupler

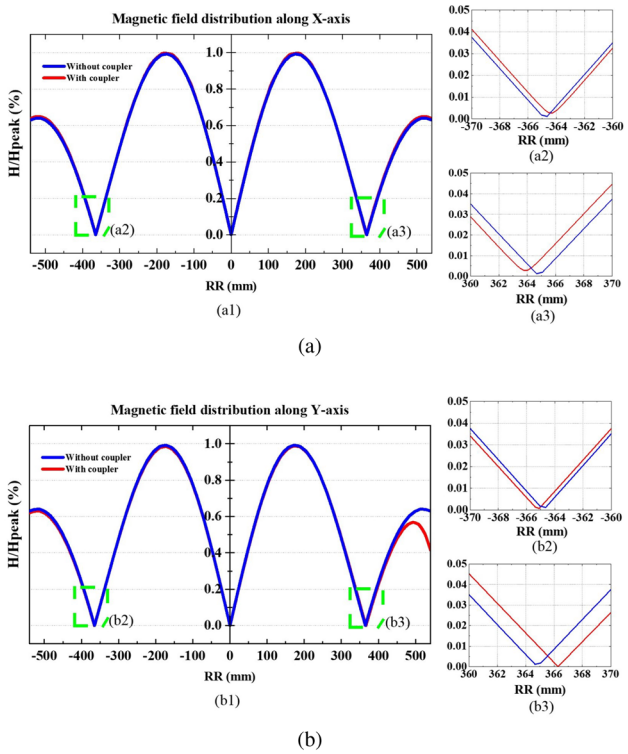

Fig. 7 (Color online) Magnetic field distributions of TM_{020}-mode along **a** *X*-axis and **b** *Y*-axis

an input coupler. The introduction of a waveguide input coupler distorts the node from a circle into an approximate ellipse, as shown in Fig. 6b. The center of the ellipse is offset toward the coupler.

This distortion is analyzed in detail in Fig. 7, where H/H_{peak} is the magnetic field normalized to the peak magnetic field inside the cavity and *RR* is the distance to the beam axis. After introducing a waveguide input coupler into the cavity, the magnetic field distribution of the TM_{020}-mode underwent an obvious transformation. As shown in Fig. 7a2, a3, the node of the magnetic field shrinks toward the beam axis by 0.5 mm along the *X*-axis. Meanwhile, Fig. 7b2, b3 illustrates that the node of the magnetic field along the *Y*-axis shifts toward the coupling port, with the entire distribution moving upward by approximately 1 mm. This change was attributed to the interaction between the coupler and cavity, which broke the rotational symmetry of the magnetic field distribution. When the coaxial slots remain rotationally symmetrical, the asymmetrical magnetic field distribution for the TM_{020}-mode may lead to leakage power into these slots, where the leaked power is ultimately absorbed by the ferrites. However, the absorption capacity of ferrites is limited by overheating issues. In a 500 MHz TM_{020}-mode RF cavity, assuming that the ferrites can handle up to 10 kW of power and the leakage rate is 10%, the maximum allowable input power is limited to 100 kW. By reducing the leakage rate to 2%, the maximum input power could be increased to 300 kW, based solely on the thermal capacity of the ferrites [20].

Two models were employed for comparison to evaluate the RF performance. One model includes a TM_{020}-mode cavity with an elliptical choke (see Fig. 8a), while the other model is a TM_{020}-mode cavity with a circular slot (see Fig. 8b). The TM_{020}-mode cavity operates at the same frequency in both models. The elliptical choke (Fig. 8a) includes an elliptical slot with its center exactly positioned at the node of the magnetic field. The dimensions of the elliptical slot are shown in Fig. 6b. Based on the theoretical analysis presented in Sect. 2, a choke length of $L = 50$ mm

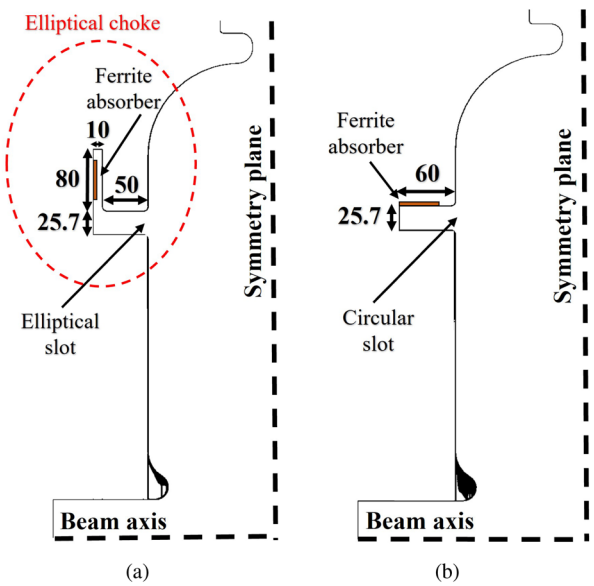

Fig. 8 (Color online) Geometry of two models: **a** elliptical slot with choke; **b** circular slot without choke

Table 1 RF parameters for two models

RF parameters	Elliptical choke	Circular slot
Working mode	TM_{020}-mode	TM_{020}-mode
Frequency (MHz)	499.7	499.7
Unloaded quality factor Q_0	66148	66166
Leakage rate P_f/P_c	1.5%	12.1%
R/Q (Ω)	71.5	72.3

was used to maximize the reflection of the TM_{020}-mode, thereby minimizing the leakage of the accelerating TM_{020}-mode. The theoretical analysis in Section II also indicates that a choke width of $W = 20 - 30$ mm balances the strong suppression of parasitic modes and preservation of the accelerating mode. Through optimizations, $W = 25.7$ mm was selected as a compromise between minimizing the leakage of the accelerating mode and deeply suppressing the parasitic modes.

The simulated RF performances of both models are summarized in Table 1. It can be observed that the cavity with a circular slot has a leakage rate of 12.1% for the accelerating TM_{020}-mode. After adding an elliptical choke to the cavity, the leakage rate was significantly reduced to 1.5%. Therefore, the elliptical choke can effectively address the leakage issue of the TM_{020}-mode cavity.

A tolerance analysis was performed by introducing an offset ΔR in the slot center position. Figure 9 shows the variation of the unloaded quality factor Q_0 and leakage rate P_f/P_c as a function of the offset ΔR in both cavities. The cavity with an elliptical choke (see Fig. 8a) maintains a higher Q_0 and lower leakage rate P_f/P_c across the entire ±3 mm offset range, compared to the cavity without the elliptical choke (see Fig. 8b). These results show that the elliptical choke not only addresses the leakage issue but also exhibits a higher tolerance to the positional offset caused by fabrication errors. To maintain a leakage rate $P_f/P_c < 5\%$, the offset ΔR must be within the range of ±0.3 mm for the proposed cavity with elliptical choke, as shown in Fig. 9b

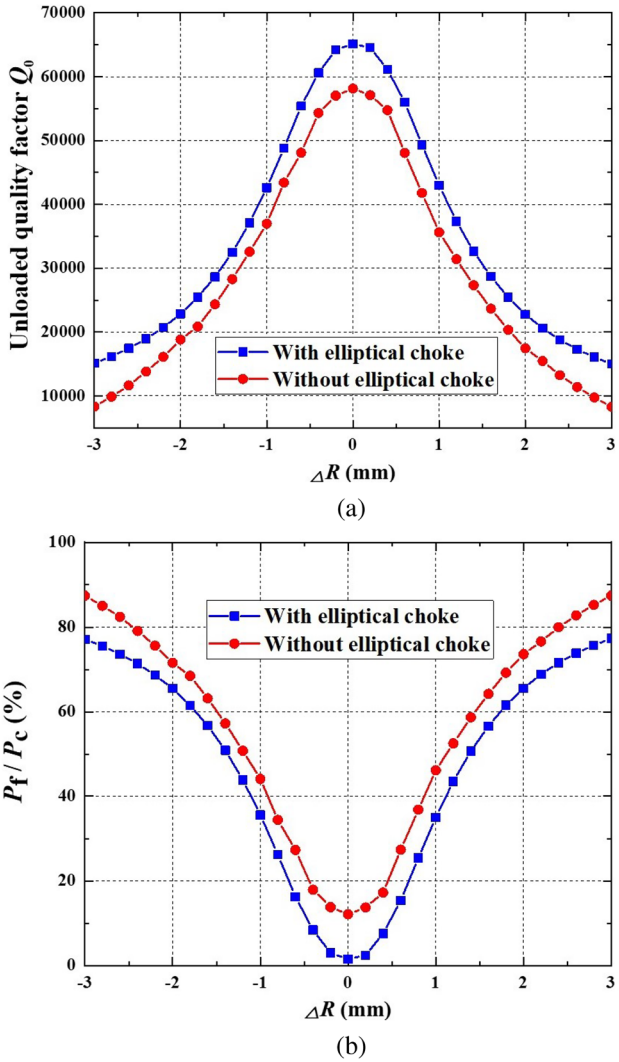

Fig. 9 (Color online) Unloaded quality factor Q_0 (**a**) and the leakage rate P_f/P_c (**b**) as a function of the slot center position offset ΔR, where P_f and P_c represent the power loss of the accelerating mode absorbed by the ferrites and the power dissipated on the cavity wall, respectively

4 Frequency tuners

Frequency tuners are typically employed as metallic plungers to adjust the frequency of the cavity. The introduction of frequency tuners can perturb the electromagnetic field distribution of the TM_{020}-mode so that some partial power of the accelerating mode leaks into the coaxial slots and is absorbed by the ferrites [16]. When inserted into the cavity, the tuner causes radial displacement of the magnetic field node, as shown in Fig. 10. This displacement results in leakage power into the coaxial slots, thereby reducing the unloaded quality factor Q_0 of the accelerating mode. Consequently, this effect increases the thermal load on the ferrite, potentially causing overheating issues.

To minimize the leakage power and ensure the required frequency tuning range, simulations were performed using one tuner, two tuners, and three tuners, respectively. The simulation results are presented in Fig. 11. The adjustable resonant frequency range was set to ±200 kHz to meet the physics requirements. When a single frequency tuner is introduced (see Fig. 10b), the node of magnetic field is further shifted along the Y-axis. To achieve a tuning range of ±200 kHz, the maximum leakage rate was calculated to be 26%, as shown in Fig. 11. This may increase the thermal load on the ferrite, potentially causing overheating issues.

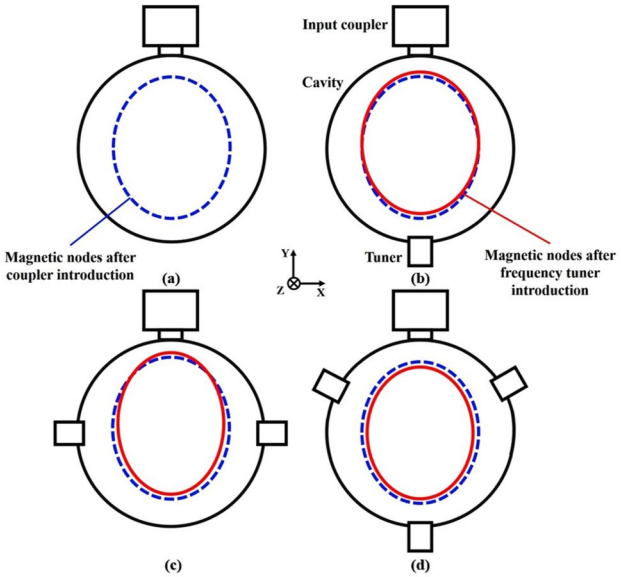

Fig. 10 (Color online) Schematics of magnetic field node deformation of the TM_{020}-mode caused by the introduction of: **a** the input coupler; **b** one tuner; **c** two tuners; and **d** three tuners

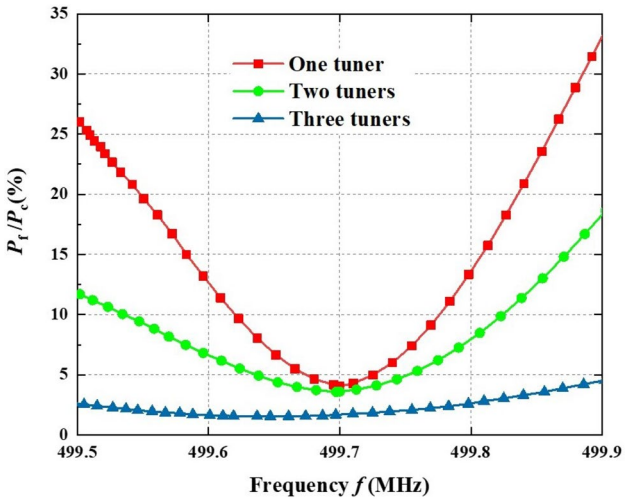

Fig. 11 (Color online) Simulated leakage rate P_f/P_c as a function of the frequency f

When two tuners are placed symmetrically (see Fig. 10c), the node of magnetic field shrinks along X-axis. It can be seen from Fig. 11 that the maximum leakage rate is simulated to be 15%. When three tuners are arranged at 120° intervals (see Fig. 10d), the node of magnetic field stays unchanged. This setup minimizes the magnetic field distortion and significantly reduces the power leakage. As shown in Fig. 11, a minimum leakage rate P_f/P_c of 1.5% can be achieved when using three symmetrically placed tuners. Throughout the tuning range of ±200 kHz, the frequency f increases linearly with the tuner insertion length, whereas Q_0 remains above 63,000 and P_f/P_c remains below 5%, as shown in Fig. 12. Therefore, three tuners with 120° rotational symmetry were selected for effective frequency tuning while minimizing the leakage rate.

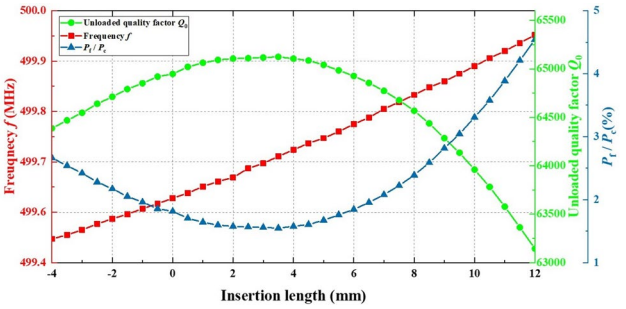

Fig. 12 (Color online) Frequency f, unloaded quality factor Q_0, and leakage rate P_f/P_c as a function of frequency tuner insertion length for three tuners

Table 2 Beam parameters of the STCF collider ring

Parameter	Value
Circumference, C (m)	865.398
Beam energy, E_0 (GeV)	2
Beam current, I_b (A)	2
Single bunch charge, q (nC)	8.34
Momentum compaction, α_p ($\times 10^{-6}$)	13.86
Bunch length, σ_z (mm)	6.96
Energy loss per turn, U_0 (keV)	541
Damping time, τ_{xy}/τ_s (ms)	21.34/10.67
Revolution frequency, f_{rev} (kHz)	346.42
Synchrotron tune, Q_s	0.0217
Betatron tunes, β_{xy} (m)	10/10

5 HOMs for TM_{020}-mode cavity with elliptical choke

When an electron beam traverses an accelerating RF cavity, harmful parasitic modes, including higher-order modes (HOMs) and TM_{010}-mode, are excited. These harmful parasitic modes can potentially degrade the beam quality by inducing longitudinal and transverse coupled-bunch instabilities (CBIs). Therefore, it is particularly important to strongly dampen these harmful parasitic modes and reduce their impedances below critical thresholds to prevent CBIs. In previous studies, we achieved a high unloaded quality factor Q_0 and a low R/Q, reducing the required detuning frequency and significantly suppressing CBIs driven by the accelerating mode [15]. In this section, a TM_{020}-mode cavity

with an elliptical choke is further optimized to ensure that all harmful parasitic modes are deeply suppressed for STCF collider rings with a beam current of up to 2 A.

The parameters of the STCF collider rings impose stringent requirements for the deep suppression of harmful parasitic modes. The longitudinal and transverse impedance thresholds can be calculated using the well-established equations with the parameters listed in Table 2 [21]:

$$Z_{\mathrm{L}}^{\mathrm{th}} = \frac{1}{f_{\parallel,\mathrm{HM}}} \cdot \frac{2E_0 Q_{\mathrm{s}}}{I_{\mathrm{b}} \alpha_{\mathrm{p}} \tau_{\mathrm{s}}}, \tag{13}$$

$$Z_{x,y}^{\mathrm{th}} = \frac{1}{f_{\mathrm{rev}}} \cdot \frac{2E_0}{I_{\mathrm{b}} \beta_{x,y} \tau_{x,y}}, \tag{14}$$

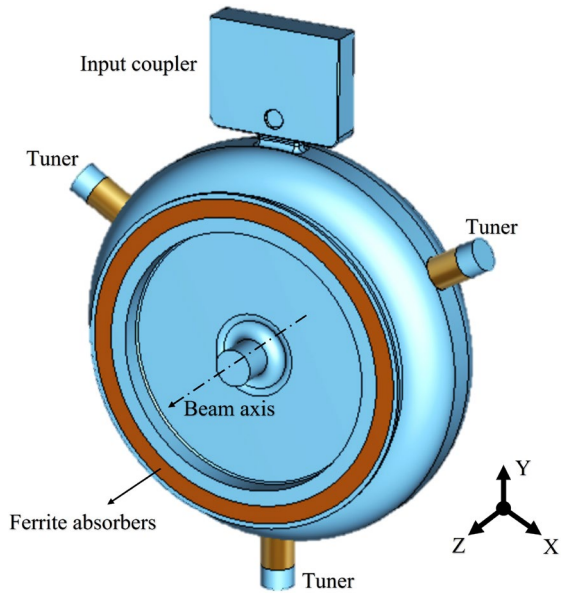

Fig. 13 (Color online) Simulation model of a TM_{020}-mode RF cavity with an elliptical choke geometry, three frequency tuners, a waveguide input coupler, and two-ring ferrites

where $Z_{\mathrm{L}}^{\mathrm{th}}$ and $Z_{x,y}^{\mathrm{th}}$ are the total longitudinal and transverse impedance thresholds; $f_{\parallel,\mathrm{HM}}$ is the frequency of the longitudinal harmful parasitic modes; E_0 is the beam energy; I_{b} is the beam current; Q_{s} is the synchrotron tune; α_{p} is the momentum compaction factor; τ_{s} is the longitudinal damping time; f_{rev} is the revolution frequency; $\tau_{x,y}$ are the transverse damping times; and $\beta_{x,y}$ are the beta functions at the cavity location.

As shown in Fig. 13, a TM_{020}-mode cavity incorporates the elliptical choke with a slot width of $W = 25.7$ mm along with three frequency tuners. The diameter of the beam pipes was chosen to be 50 mm, so the corresponding cutoff frequencies of the TE_{11} and TM_{01} modes in the beam pipes were 1.75 GHz and 2.30 GHz, respectively. The optimized RF parameters of the TM_{020}-mode are listed in Table 3.

Through optimization, the magnetic field nodes of the harmful parasitic modes were separated from those of the accelerating mode within the cavity, as shown in Fig. 14. This spatial separation allows the harmful parasitic modes to propagate through the elliptical choke and be effectively damped by the ferrites.

For the longitudinal impedance Z_{L} and transverse impedance $Z_{x,y}$, the following definitions are used:

Table 3 RF parameters for an optimized TM_{020}-mode cavity

RF parameters	Value
Working mode	TM_{020}-mode
Frequency (MHz)	499.7
Unloaded quality factor Q_0	66148
Leakage rate $P_{\mathrm{f}}/P_{\mathrm{c}}$	1.5%
R/Q (Ω)	71.5
Shunt impedance R_{a} (MΩ)	4.7
$E_{\mathrm{peak}}/E_{\mathrm{acc}}$	2.11
$B_{\mathrm{peak}}/E_{\mathrm{acc}}$ (mA/V)	2.48

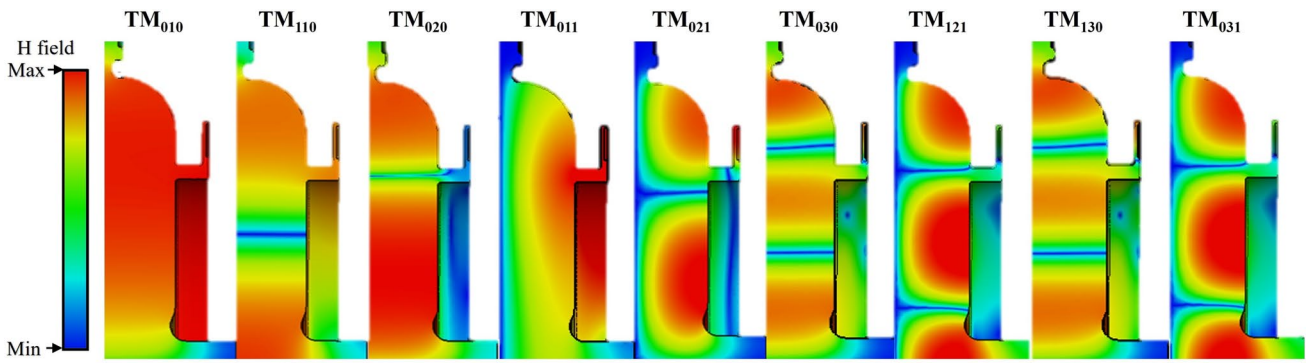

Fig. 14 (Color online) Magnetic field distributions of the TM_{020}-mode and harmful parasitic modes in the cavity with elliptical choke

$$Z_{\mathrm{L}} = \frac{R(r=0)}{Q} \cdot Q_{\mathrm{l}}(r=0)\ (\Omega), \tag{15}$$

$$Z_{x,y} = \frac{R(r)}{Q} \cdot Q_{\mathrm{l}} \cdot \frac{1}{kr^2}\ (\Omega/\mathrm{m}), \tag{16}$$

$$\frac{R(r)}{Q} = \frac{V(r)^2}{2\omega U}\ (\Omega), \tag{17}$$

where $k = \omega/c$ is the wave number, ω is the angular frequency, c is the speed of light, r is the radial offset from the cavity axis, $V(r)$ is the cavity voltage, and U is the stored energy in the cavity.

As shown in Fig. 15, the longitudinal and transverse impedances of the harmful parasitic modes in the TM_{020}-mode cavity are calculated using CST Particle Studio and Microwave Studio [22]. Almost all impedances were below the threshold. This indicates that all harmful parasitic modes were deeply suppressed, meeting the requirements of the STCF collider rings with a beam current of up to 2 A.

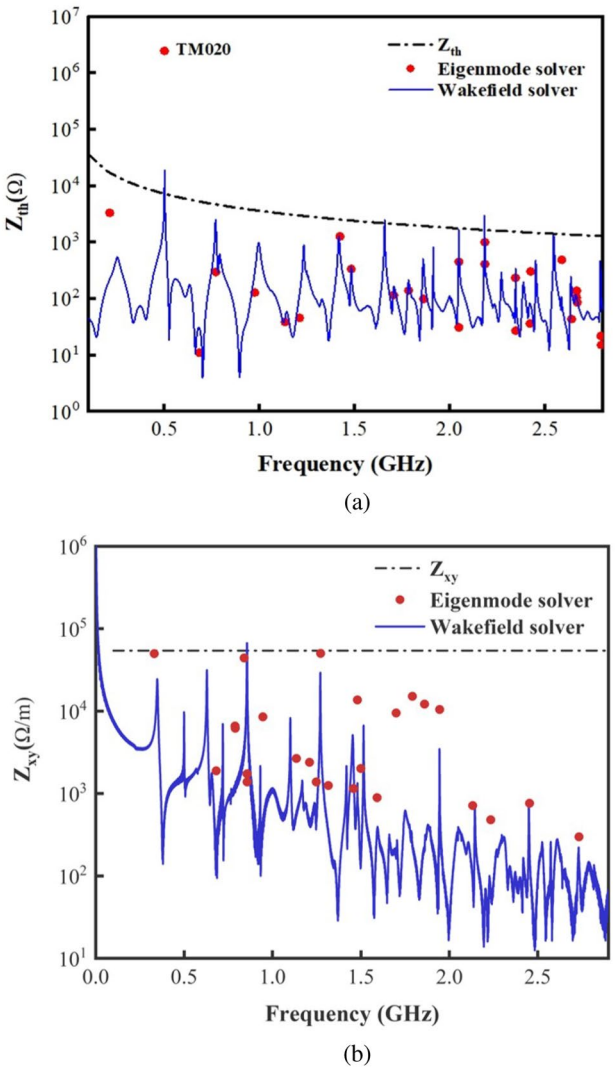

Fig. 15 (Color online) Calculated longitudinal (**a**) and transverse (**b**) impedance with different frequencies

6 Multipacting analysis

Multipacting is a phenomenon of resonant electron multiplication when an RF cavity with an input coupler is used for high-power conditioning. This occurs when RF fields sustain electrons on resonant trajectories, causing repeated wall impacts and secondary electron emissions that drive exponential electron multiplication. If the impact energy and material-dependent secondary electron yield (SEY) favor emission, exponential electron multiplication occurs, as described by the secondary electron effect in Eq. (18). When $\alpha > 0$ in Eq. (18), the number of particles increases exponentially over time, which is equivalent to the relationship in Eq. (19). A key parameter, SEY, is introduced, and its definition is provided in Eq. (20). When SEY> 1, secondary electron multiplication occurs [23].

$$\log N(t) = \log N_0 + \alpha t, \tag{18}$$

$$N_{\mathrm{e},m} = N_0 (SEY)^m, \tag{19}$$

$$SEY = \frac{n_{\mathrm{e}}}{n_{\mathrm{c}}} = \frac{I_{\mathrm{e}}}{I_{\mathrm{c}}}, \tag{20}$$

where N_0 is the initial number of particles, α is a growth factor, $N_{\mathrm{e},m}$ is the number of electrons after m times of

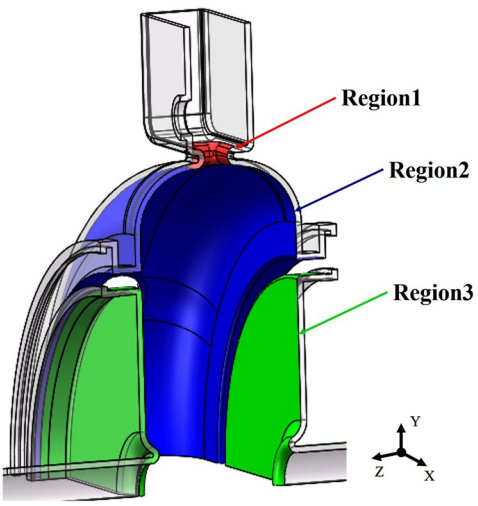

Fig. 16 (Color online) Modeling of the optimized cavity for multipacting simulations

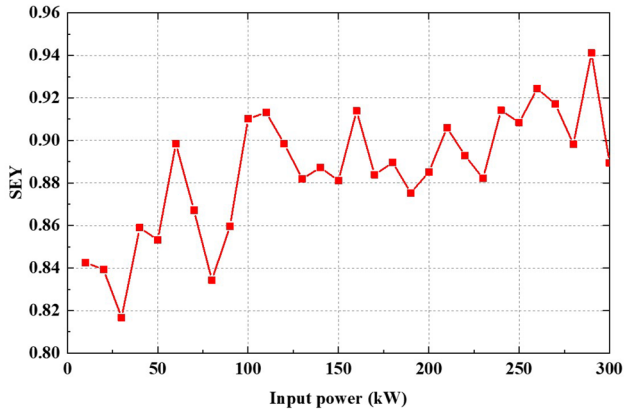

Fig. 17 (Color online) Simulated SEY as a function of the input power for the coupling port area

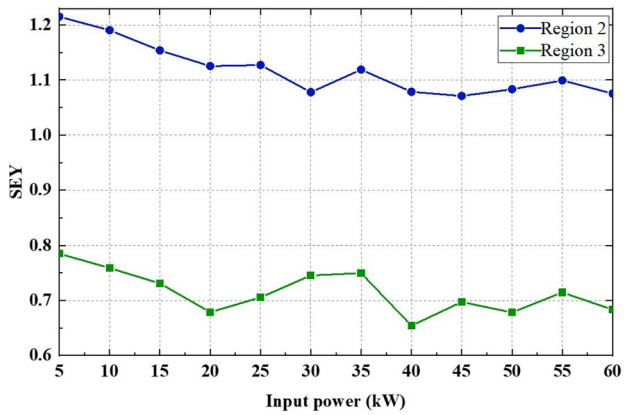

Fig. 18 (Color online) Simulated SEY as a function of the input power for the inner face of the optimized cavity

secondary electron emission, m is the times of secondary electron emission, SEY is the secondary emission yield, n_e and n_c are the secondary and primary electron numbers, respectively, and I_e and I_c are the secondary and primary currents, respectively.

Multipacting simulations were performed using the CST Particle Studio [22]. As shown in Fig. 16, Region 1 corresponds to the coupling port area, whereas Region 2 and Region 3 represent the inner face of the optimized cavity. For the coupling port area, the input power was swept from 10 kW to 300 kW at a step of 10 kW, and the corresponding SEY are plotted in Fig. 17. As shown in Fig. 17, SEY remains below 1, indicating multiplication does not occur in the coupling port area. For the inner face of the cavity, the input power was swept from 5 kW to 60 kW at a step of 5 kW. As shown in Fig. 18, the simulated SEY in Region 2 is slightly above 1, which can be readily eliminated through high-power conditioning, while the simulated SEY of in Region 3 remains below 1, indicating multipacting doesn't occur at all. Therefore, these simulations demonstrate that there is no risk of multipacting for the optimized cavity when it is used for high-power conditioning.

7 Thermomechanical analysis

When tens of kW RF power is transmitted into the optimized TM_{020}-mode cavity, the cavity undergoes mechanical deformation, resulting in frequency shifts and degrading the RF performance of the accelerating mode. Therefore, thermomechanical analysis must be performed for this cavity.

7.1 Thermal load calculation

The thermal load of the TM_{020}-mode cavity arises from two primary sources: the power loss on the cavity surface associated with generating the accelerating voltage and the power absorbed by the ferrites. The accelerating voltage in the cavity V_a is defined as:

$$V_a = \sqrt{R_a P_c}, \tag{21}$$

where P_c is the power loss on the cavity surface and R_a is the shunt impedance for the accelerating mode. For our design, an accelerating voltage of $V_a = 500$ kV corresponds to a surface power loss of $P_c = 55$ kW.

The power absorbed by the ferrites includes both the leakage power from the TM_{020}-mode and the power of the harmful modes excited by the beam. Among them, the maximum leakage rate of the TM_{020}-mode within the tuning range is approximately 5%, corresponding to a leakage power of 2.75 kW absorbed by the ferrites.

The power of the harmful parasitic modes excited by the beam in the cavity is calculated using the following equations [24]:

$$P_{HM} = k_{HM} \cdot q \cdot I_0, \tag{22}$$

$$k_{HM} = k_t - k_0, \tag{23}$$

$$k_0 = \frac{\omega_0}{4} \cdot \frac{R}{Q} \cdot e^{-\omega_0^2 \sigma_t^2}, \tag{24}$$

$$k_t = -\int_{-\infty}^{\infty} W_{\parallel}(s)\lambda(s)\,\mathrm{d}s, \tag{25}$$

where P_{HM} is the power of the harmful parasitic modes, k_{HM} is the loss factor of the harmful parasitic modes, q is the bunch charge, I_0 is the beam current, k_t is the total loss factor, k_0 is the loss factor of the accelerating mode, ω_0 is

the angular frequency of the accelerating mode, R/Q is the ratio of the shunt impedance to the unloaded quality factor for the accelerating mode, σ_t is the bunch length in time, $W_{\parallel}(s)$ is the longitudinal wake function, and $\lambda(s)$ is the bunch distribution. From Table 2, the bunch length in time is given by $\sigma_t = \sigma_z/c = 23.2$ ps, where $\sigma_z = 6.96$ mm is the bunch length, and c is the speed of light. Using CST wavefield solver [22], $k_t = 0.45$ V/pC, $k_0 = 0.05$ V/pC, and $k_{HM} = 0.39$ V/pC are obtained. By substituting $q = 8.34$ nC and $I_0 = 2$ A into Eq. (22), the power of harmful parasitic modes excited by the beam is calculated to be $P_{HM} = 6.6$ kW

When a leakage rate of 5% is assumed, the leakage power from the accelerating mode is calculated to be approximately 2.75 kW. In this case, the total power absorbed by the ferrites was calculated to be 9.35 kW.

7.2 Mechanical design

Using the optimum dimensions in Sects. 3 and 4, a mechanical TM_{020}-mode cavity was modeled. As shown in Fig. 19, the brown and gray regions represent components made of oxygen-free high-conductivity copper (OFHC) and stainless steel (SS), respectively. The cavity comprises two beam pipe flanges, twelve ferrite modules, two ferrite flanges, two end plate flanges, a main body, two nose cone plates, and structural supports. The main body was machined from OFHC and brazed to SS end plates, forming internal cooling water channels within the cavity (see Fig. 20a). Each nose cone plate consists of two OFHC components brazed together to create an internal water-cooling passage (see Fig. 20b) and subsequently brazed to an SS ferrite flange. Each ferrite flange features six openings to install six ferrite modules. Each ferrite module is composed of eighty ferrite blocks (16 mm × 16 mm × 2 mm), a copper base, and an SS flange, as shown in Fig. 20c). Vacuum sealing between the ferrite modules, ferrite flanges, and end plate flanges was achieved using metal O-rings or gaskets.

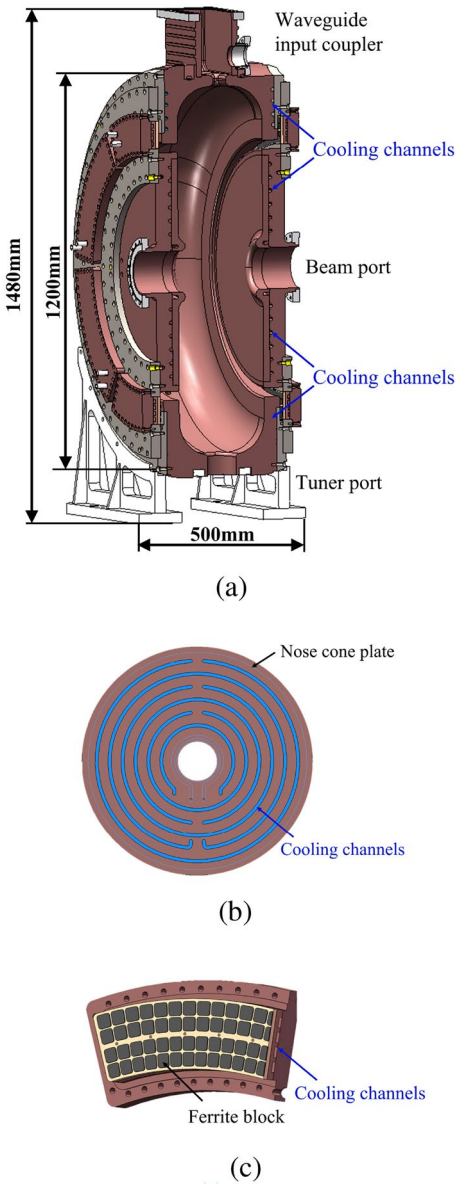

Fig. 20 (Color online) Mechanical model of the cavity: the layout of cooling channels for the main body (**a**), each nose cone plate (**b**), and each ferrite module (**c**)

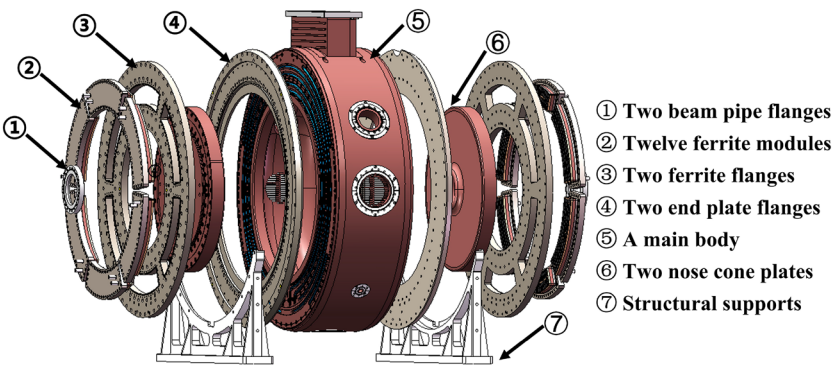

Fig. 19 (Color online) Structural overview of the TM_{020} -mode cavity

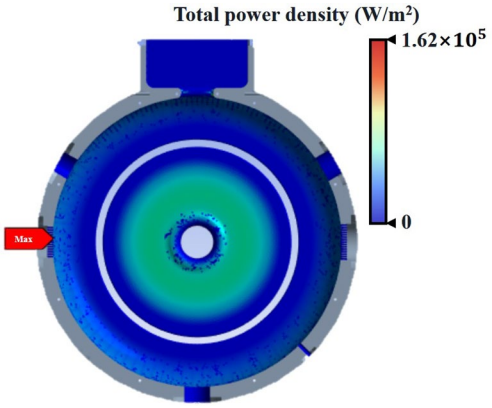

Fig. 21 (Color online) The power density distribution for the cavity with a thermal load of $P_c = 55$ kW

7.3 Thermal analysis

To assess the mechanical robustness of the cavity, a coupled thermal-structural analysis was conducted using ANSYS Mechanical [19]. A thermal load of $P_c = 55$ kW (corresponding to an accelerating voltage of 500 kV) was utilized in the following analysis, as shown in Fig. 21. For the cooling system shown in Fig. 20, the flow rate of 10–15 L/min (corresponding to an average velocity of 3 m/s) and an inlet water temperature of 24 °C are assumed. The heat transfer coefficient on the cooling channel walls was estimated to be 1.5 W/(cm^2 · K). The steady-state temperature field obtained from the thermal analysis was subsequently used as an input for the structural stress analysis to assess the effects of thermal expansion. In addition, atmospheric pressure was applied as an external mechanical load.

The simulated temperature distribution is presented in Fig. 22a, and the von Mises stress distributions for different components are presented in Fig. 22b, c. The maximum temperature of 42.31 °C occurs on the inner surface of the end plate. The peak von Mises stress was 82.07 MPa in the SS region of the flange and 60.85 MPa in the main body with OFHC. Both values were within the acceptable limits for reliable operation. The maximum total deformation of 0.16 mm occurred on the flange, as shown in Fig. 22d. Using this deformation, the resonant frequency of the accelerating TM_{020}-mode was simulated to shift by less than −100 kHz under high-power testing. Such a frequency shift can be compensated back through three tuners inside the cavity. The thermal analysis showed that the mechanical design of the cavity was sufficiently robust.

A similar thermal analysis was also performed for a single ferrite module. The total power absorbed by the ferrites was calculated to be 9.35 kW; thus, a power of 12 kW was utilized for the maximum heat load of the ferrites, leaving 2.65 kW as a safety margin. In this situation, a power of 1 kW was applied to each ferrite module, resulting in a total of 12 kW across all twelve ferrite modules. When the field distributions at the slots for the accelerating mode are employed for the thermal analysis, the heat load is distributed unevenly on a single ferrite module, as shown in Fig. 23a.

The simulated temperature distributions of the ferrite module are shown in Fig. 23b, c, while the von Mises stress distribution is presented in Fig. 23d. The temperature of the ferrite blocks increases from 24 °C to a maximum of 64.7 °C, resulting in a temperature rise of 40.7 °C. Given the Curie temperature of 100 °C for ferrites, such a high temperature is acceptable. The

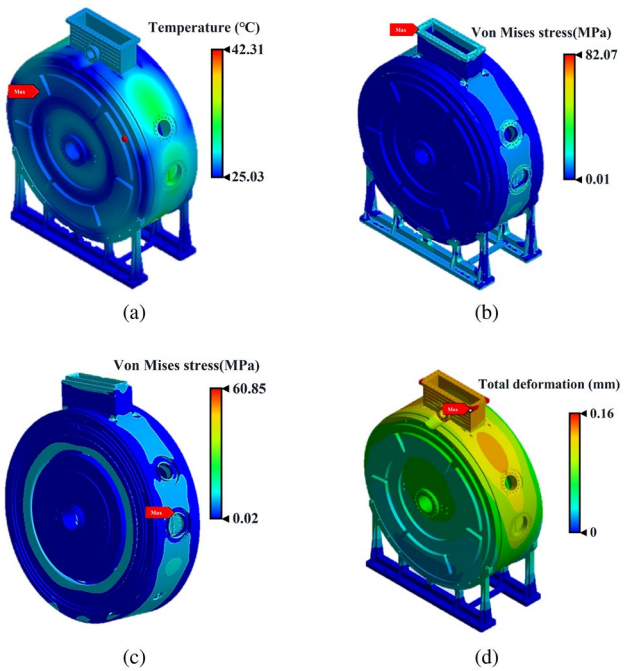

Fig. 22 (Color online) The coupled thermal-structural analysis for the whole cavity: **a** temperature distribution, **b** von Mises stress distribution in the whole cavity, **c** von Mises stress distribution in the OFHC parts, and **d** total deformation in the whole cavity

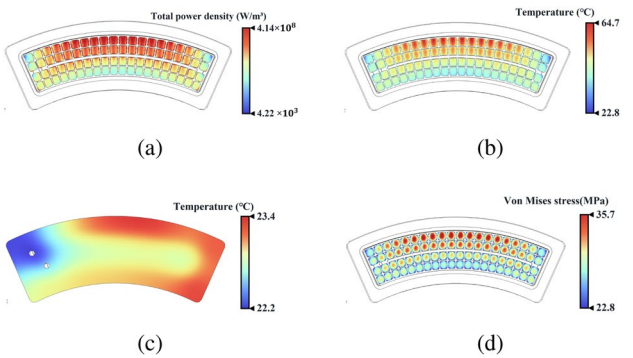

Fig. 23 (Color online) The coupled thermal-structural analysis for a single ferrite module: **a** power density distribution and **b** temperature distribution in the ferrite blocks; **c** temperature distribution in the ferrite module flange and **d** von Mises stress distribution in the ferrite blocks

peak von Mises stress was 35.7 MPa at the bonding interface between the ferrite blocks and copper base. Considering that the typical tensile strength of Ni-Zn ferrites is 50 MPa, the simulated von Mises stress remains approximately 70% of the tensile limit for ferrite blocks. Therefore, the mechanical design of the ferrite module exhibited good robustness through thermal analysis.

8 Summary

A 500 MHz TM_{020}-mode cavity with an elliptical choke was designed in detail in this study. By employing an elliptical choke, the leakage power of the accelerating mode caused by the waveguide coupler was significantly reduced to approximately 1.5%. Additionally, an analysis of the leakage power caused by the frequency tuners was conducted. All harmful parasitic modes can be strongly suppressed through optimizations of the inner shape of the cavity with a large beam pipe, meeting the requirements of the STCF collider rings with a beam current of up to 2 A. The mechanical design and thermal analysis of the TM_{020} -mode cavity were completed and presented, demonstrating the feasibility of the design. The fabrication of this cavity is currently underway. Benchmark measurements are expected to be performed with the results from simulations to further optimize the cavity by the end of 2025.

References

1. C.G. Schroer, H.C. Wille, O.H. Seeck et al., The synchrotron radiation source PETRA III and its future ultra-low emittance upgrade PETRA IV. Eur. Phys. J. Plus **137**, 1312 (2022). https://doi.org/10.1140/epjp/s13360-022-03517-6
2. P. Zhang, X. Hao, T. Huang et al., A 166.6 MHz superconducting rf system for the HEPS storage ring. J. Phys. Conf. Ser. **874**, 012091 (2017). https://doi.org/10.1088/1742-6596/874/1/012091
3. Q. Gu, L.X. Chen, M. Chen et al., RF system for the SSRF Booster synchrotron. *Proceedings European Particle Accelerator Conference*. EPAC08, 754–756 (2008)
4. V.N. Volkov, N.G. Gavrilov, E.I. Gorniker et al., 178 MHz cavity with HOM damping for the DFELL storage ring. Vopr. Atom. Nauki i Tekhn. **2**, 64–66 (2004)
5. Z. Li, K. Ye, L. Yang et al., Electromagnetic field compensation to attenuate energy leakage in TM020 mode damped cavity. Nucl. Eng. Technol. **57**(3), 103256 (2025). https://doi.org/10.1016/j.net.2024.10.018
6. A. Yamamoto, Superconducting RF cavity development for the international linear collider. IEEE Trans. Appl. Supercond. **19**(3), 1387–1393 (2009). https://doi.org/10.1109/TASC.2009.2018756
7. F. Zimmermann, M. Benedikt, A. S. Müller et al., The future circular collider study. *Proceedings 11th International Particle Accelerator Conference* IPAC2020 (2020). https://doi.org/10.18429/JACOW-IPAC2020-MOVIR01
8. K. Papke, A.A. Carvalho, C. Zanoni et al., Design studies of a compact superconducting rf crab cavity for future colliders using Nb/Cu technology. Phys. Rev. Accel. Beams **22**, 072001 (2019). https://doi.org/10.1103/PhysRevAccelBeams.22.072001
9. R.L. Ives, M. Read, T. Bui et al., High efficiency, low cost, RF sources for accelerators and colliders. J. Instrum. **18**, T05003 (2023). https://doi.org/10.1088/1748-0221/18/05/T05003
10. M. Achasov, X.C. Ai, L.P. An et al., STCF conceptual design report (Volume 1): physics & detector. Front. Phys. **19**(1), 14701 (2024). https://doi.org/10.1007/s11467-023-1333-z
11. X.C. Ai, L.P. An, S.Z. An et al., Conceptual design report of the Super Tau-Charm Facility: the accelerator. Nucl. Sci. Tech. **36**, 242 (2025). https://doi.org/10.1007/s41365-025-01833-x
12. Y. Wei, Z. Huang, Z. Cao et al., Preliminary design of a 500 MHz normal-conducting cavity for main rings of Super Tau-Charm Facility. *Proceedings 15th International Particle Accelerator Conference IPAC2024*, Nashville, TN, 1467–1469 (2024). https://doi.org/10.18429/JACoW-IPAC2024-TUPR23
13. H. Ego, J. Watanabe, S. Kimura et al., Design of a HOM-damped RF cavity for the SPring-8-II storage ring. *Proceedings 11th Annual Meeting of Particle Accelerator Society of Japan*. PASJ2014, Aomori, 237–241 (2014)
14. J.Y. Zhu, X. Li, J.B. Yu et al., A low-frequency normal conducting cavity with higher-order mode damping for fourth-generation synchrotron radiation sources. Rev. Sci. Instrum. **94**(12), 123304 (2023). https://doi.org/10.1063/5.0169598
15. A. Burov, Coupled-beam and coupled-bunch instabilities. Phys. Rev. Accel. Beams **21**(11), 114401 (2018). https://doi.org/10.1103/PhysRevAccelBeams.21.114401
16. T. Yamaguchi, N. Yamamoto, D. Naito et al., Design and low-power measurement of 1.5 GHz TM020-type harmonic cavity for KEK future synchrotron light source. Nucl. Instrum. Methods Phys. Res. Sect. A **1053**, 168362 (2023). https://doi.org/10.1016/j.nima.2023.168362
17. T.S. Shintake, The choke mode cavity. Jpn. J. Appl. Phys. **31**(11A), L1567 (1992). https://doi.org/10.1143/JJAP.31.L1567
18. H. Zha, J. Shi, H. Chen et al., Choke-mode damped structure design for the Compact Linear Collider main linac. Phys. Rev. ST Accel. Beams **15**(12), 122003 (2012). https://doi.org/10.1103/PhysRevSTAB.15.122003
19. ANSYS, ANSYS engineering simulation software. https://www.ansys.com/
20. T. Inagaki, H. Tanaka, T. Ohshima et al., High-power model design of the 1.5 GHz TM020-type harmonic cavity for the future synchrotron light sources. *Proceedings 14th International Particle Accelerator Conference IPAC2023*, 188–192 (2023). https://doi.org/10.18429/JACOW-IPAC2023-WEODC3
21. A.W. Chao, Physics of collective beam instabilities in high energy accelerators. Wiley Series in Beam Physics and Accelerator Technology, Wiley, New York (1993)
22. CST Studio Suite, https://www.cst.com/
23. X. Hao, J. Zhu, X. Li et al., A study of the electromagnetic fields leakage in TM020 mode HOM-damped cavity. Nucl. Eng. Technol. **57**(11), 103717 (2025). https://doi.org/10.1016/j.net.2025.103717
24. G.V. Stupakov, Wake and impedance. *Proceedings 2000 Particle Accelerator Conference PAC2000*, Chicago, IL, USA, AIP Conference Proceedings **592**, 205–230 (2001). https://doi.org/10.1063/1.1420417